





# Natriuretic peptide receptor-C perturbs mitochondrial respiration in white adipose tissue

Shi-Jin Li<sup>1,2,\*</sup>, Jin-Qiu Wei<sup>1,\*</sup>, Yuan-Yuan Kang<sup>1</sup>, Rui-Qi Wang<sup>1,3</sup>, Wu-Wei Rong<sup>1</sup>, Jia-Jia Zhao<sup>1</sup>, Qian-Wan Deng<sup>1</sup>, Ping-Jin Gao<sup>1</sup>, Xiao-Dong Li<sup>1,\*</sup>, and Ji-Guang Wang<sup>1</sup>

<sup>1</sup>Department of Cardiovascular Medicine, Department of Hypertension, State Key Laboratory of Medical Genomics, Shanghai Key Laboratory of Hypertension, Shanghai Institute of Hypertension, Ruijin Hospital, Shanghai Jiao Tong University School of Medicine, Shanghai, China; <sup>2</sup>State Key Laboratory of Membrane Biology, Institute of Molecular Medicine, College of Future Technology, Peking University, Beijing, China; and the <sup>3</sup>Shanghai Institute of Materia Medica, Chinese Academy of Sciences, Shanghai, China

**Abstract** Natriuretic peptide receptor-C (NPR-C) is highly expressed in adipose tissues and regulates obesity-related diseases; however, the detailed mechanism remains unknown. In this research, we aimed to explore the potential role of NPR-C in cold exposure and high-fat/high-sugar (HF/HS) diet-induced metabolic changes, especially in regulating white adipose tissue (WAT) mitochondrial function. Our findings showed that NPR-C expression, especially in epididymal WAT (eWAT), was reduced after cold exposure. Global *Npr3* (gene encoding NPR-C protein) deficiency led to reduced body weight, increased WAT browning, thermogenesis, and enhanced expression of genes related to mitochondrial biogenesis. RNA-sequencing of eWAT showed that *Npr3* deficiency enhanced the expression of mitochondrial respiratory chain complex genes and promoted mitochondrial oxidative phosphorylation in response to cold exposure. In addition, *Npr3* KO mice were able to resist obesity induced by HF/HS diet. *Npr3* knockdown in stromal vascular fraction (SVF)-induced white adipocytes promoted the expression of proliferator-activated receptor gamma coactivator 1 $\alpha$  (PGC1 $\alpha$ ), uncoupling protein one (UCP1), and mitochondrial respiratory chain complexes. Mechanistically, NPR-C inhibited cGMP and calcium signaling in an NPR-B-dependent manner but suppressed cAMP signaling in an NPR-B-independent manner. Moreover, *Npr3* knockdown induced browning via AKT and p38 pathway activation, which were attenuated by *Npr2* knockdown. Importantly, treatment with the NPR-C-specific antagonist, AP-811, decreased WAT mass and increased PGC-1 $\alpha$ , UCP1, and mitochondrial complex expression.  Our findings reveal that NPR-C deficiency enhances mitochondrial function and energy expenditure in white adipose tissue, contributing to improved metabolic health and resistance to obesity.

**Supplementary key words** browning • mitochondrial complex • natriuretic peptide receptor C • obesity • white adipose tissue

The increasing incidence of obesity and its associated metabolic disorders has intensified the search for molecular targets capable of regulating adipose tissue (AT) function and energy balance. Excess nutrients contribute to the accumulation of cholesterol and triglycerides in AT, which leads to the hypertrophy of white adipose tissue (WAT), including subcutaneous WAT (sWAT) and visceral WAT (1). Notably, accumulating evidence suggests that visceral WAT is more closely associated with metabolic dysfunction compared to sWAT (2, 3). In mice, the most well studied visceral WAT is the peri-gonadal white adipose tissue, is commonly referred to as epididymal WAT (eWAT) in males (4).

Natriuretic peptides (NPs), such as atrial natriuretic peptide (ANP), B-type natriuretic peptide (BNP), and C-type natriuretic peptide (CNP) are highly expressed in AT and affect AT metabolism through their interactions with NP receptors (NPRs) (5). ANP and BNP activate thermogenic energy expenditure through activating NPR-A/cyclic GMP (cGMP) pathway (6, 7). CNP regulates thermogenesis and adipogenesis by binding to both NPR-B and NPR-C concomitantly (8). It has been reported that NPR-C levels in AT of obese hypertensive patients are much higher than those in patients with normal blood pressure patients (9). NPR-C deficiency protects against insulin resistance and diet-induced obesity in obese mice (7). However, the conventional perception that NPR-C acts solely as a receptor for NPs' clearance has been refuted by growing evidence showcasing its diverse effects on

\*These authors contributed equally to this work.

\*For correspondence: Xiao-Dong Li, [flylxd@163.com](mailto:flylxd@163.com).

various cells and organs, as well as its specific intracellular mechanisms of action. (10). Recent studies revealed that apart from coupling with the inhibitory G (Gi) protein, (11) NPR-C binds directly with NPR-A or NPR-B to form heterodimers, indicating the pivotal role of NPR-C in regulating adipose metabolism through the modulation of NPs and receptors levels (12). Notably, NPR-C expression is higher in mice eWAT compared to sWAT and peri-renal AT (13). However, the detailed mechanism of NPR-C in the regulation of WAT metabolism is not fully understood.

The mitochondrial dysfunction contributes to WAT remodeling and energy balance (14). Beige adipocytes reside within WAT and emerge in response to cold exposure and display the capacity for adaptive thermogenesis, which is regulated by mitochondria (15). Mitochondrial respiration chain fuels multiple cellular biological processes through the transfer of electrons and the production of ATP. In this investigation, we discovered that deficiency of NPR-C promotes WAT thermogenesis and attenuates high-fat/high-sugar (HF/HS)-induced obesity and metabolic dysfunction by improving mitochondrial respiration. Mechanistically, down-regulation of NPR-C leads to the over-activation of NPR-B/cGMP and increased phosphorylation of AKT and p38 signaling. Therefore, inhibiting NPR-C signaling may be a potential target for treating metabolic diseases.

## MATERIALS AND METHODS

### Animals

The C57BL/6J wild-type (WT) mice were accommodated in an environment with a 12-h-light/12-h-dark cycle. The mice had free access to standard chow and water. *Npr3* KO (KO) mice were constructed by Cyagen Biotechnology. In the cold exposure model, we randomly assigned eight-week-old WT and KO male mice into two groups: room temperature (RT) and cold exposure (Cold). The mice in the Cold group were individually placed in 4°C environment for a period of 72 h. For the HF/HS model, four-week-old WT or KO male mice were randomly grouped and fed an HF/HS diet (D12266B, Research Diets, 32 kcal% fat) for 14 weeks. In the AP-811 treatment study, male eight-week-old WT mice received intraperitoneal injections of AP-811 (0.4 mg/kg/d) or 0.9% NaCl for seven days.

All animal study protocols were approved by the Committee on Ethics for Animal Experiments at Shanghai Jiao Tong University School of Medicine, in compliance with the Guide for the Care and Use of Laboratory Animals.

The study protocol was approved by the Committee on Human Research at Ruijin Hospital, Shanghai Jiao Tong University School of Medicine. All participants provided written informed consent.

### Metabolic studies

The mice were individually accommodated in the PhenoMaster system (TSE Systems Inc) for 24 h to adapt to the environment. Then the mice were housed for a consecutive

48 h with unrestricted access to food and water. Measurements of respiratory exchange ratio (RER),  $\text{VO}_2$ , and  $\text{VCO}_2$  were taken every 27 min. RER was determined using the formula  $\text{RER} = \text{VCO}_2/\text{VO}_2$ , and energy expenditure was calculated using the equation:  $\text{EE} = 1.44 (3.941 \times \text{VO}_2 + 1.106 \times \text{VCO}_2)$ . The system also recorded spontaneous locomotor activity, as well as food and water intake.

### Magnetic resonance imaging (MRI) of body composition

MesoMR23-060H-I medium-sized NMR analysis and imaging system (Suzhou Niumar Analytical Instruments Co., LTD.) was used. The parameters were a resonant frequency 23.313 MHz, magnet strength 0.55 T, a coil diameter 60 mm. Mice were anesthetized and placed in a carrier bed. In the body composition test, mice were placed into the body fat carrier bed and a 60 mm probe coil was used for detection.

### Glucose tolerance test (GTT) and insulin tolerance test (ITT)

To conduct the GTT analysis, mice underwent an overnight fast before receiving glucose (2 g/kg, i.p.). For the ITT analysis, mice underwent 4 h fast before receiving insulin (0.5 IU/kg, i.p.). Blood glucose was measured at 0, 15, 30, 60, 90, and 120 min using a Roche Accu-Chek Aviva glucose monitor system (Roche, Switzerland). The area under the curve was determined using GraphPad Prism software.

### H&E staining and immunofluorescent

Adipose tissues underwent fixation in 4% paraformaldehyde at room temperature for a period of 48 h. The tissues were then embedded and sliced into 5  $\mu\text{m}$ , and then subjected to deparaffinization and rehydration through a series of graded ethanol-water solutions. Subsequently, the sections were stained using hematoxylin and eosin (H&E). In immunofluorescence staining, the sections were treated with primary antibodies overnight at 4°C, targeting NPR-C (Santa Cruz Biotechnology, sc-515449, 1:100) and UCPI (Abcam, ab10983, 1:100). Following this, the sections were washed with PBS and incubated with fluorochrome-conjugated secondary antibody (1:200) for 1 h. DAPI was used to stain nuclei. Imaging was performed using a Carl Zeiss Axio Imager M2 microscope (Carl Zeiss Corporation, Germany) and analyzed by Image-Pro Plus (Media Cybernetics, USA).

### Cell culture

The WAT was collected from 6-week-old male C57BL/6J mice, finely chopped, and then digested at 37°C using collagenase II (Sigma-Aldrich) for 45 min. The resulting cell suspension underwent filtration, centrifugation, and resuspension in growth medium (DMEM/F12 1:1 + 1% penicillin/streptomycin + 10% FBS). The stromal vascular fraction (SVF) cells were cultured until they reached confluence. Subsequently, differentiation was initiated using a mixture of 1  $\mu\text{M}$  dexamethasone, 0.5 mM IBMX, and 10  $\mu\text{g}/\text{ml}$  insulin. After 2 days of induction, the culture medium was changed to include 10  $\mu\text{g}/\text{ml}$  insulin. On the fourth day of differentiation, the cells were transitioned to a growth medium containing 10% FBS, and the medium was refreshed every other day until the adipocytes were ready for use on the sixth day. SVF-induced white adipocytes were rendered quiescent by incubating in DMEM/F12 without FBS for 24 h and

subsequently exposed to CL316,243 (100 nM) for 6 h. SVF-induced white adipocytes were infected with sh*Npr3* or sh*Npr2* at a multiplicity of infection (MOI) of 20 for 48 h. The short hairpin RNAs (shRNAs) were synthesized by GEN-ECHEM (Shanghai, China). The sequence targeting the mouse scramble RNA control (shCt1): TTCGTGGTGACTAGACACCAG; sh*Npr3*: GACCAGTGGAGACTACGGCTTT; sh*Npr2*: GCCATCATTCTACAGGAAATA. SVF-induced white adipocytes were treated with CL316,243 (MCE, HY-116771A, 100 nM), MK2206 (Selleck, SI078, 10 μM), and SB203580 (MCE, HY-10256, 10 μM).

### Oil Red O staining

SVF cells were transfected with shRNA under the previously mentioned conditions. Upon reaching confluence, induced differentiation was performed using the established protocol. Mature adipocytes were washed with PBS and stained using the Oil Red O staining kit (Beyotime, C0158s).

### RNA isolation and quantitative PCR (qPCR)

To obtain total RNA, tissues and cultured cells were subjected to TRIzol (Invitrogen) according to the manufacturer's instructions. Then the suspension was centrifuged, and the supernatant was collected. Trichloromethane was added to the supernatant and mixed thoroughly. The suspension was centrifuged again, and isopropanol was added to precipitate the RNA. Next, RNA precipitate was washed with 75% ethanol and dissolved in DEPC water. Using a Nano Drop Spectrophotometer (Thermo Fisher Scientific) to measure the concentration. Aliquots of total RNA were reverse transcribed into cDNA using the Prime Script RT Master Mix Kit (EZBioscience). qPCR was conducted utilizing SYBR Premix Ex Taq kits with Rox (Vazyme, Nanjing, China) on the StepOne Plus System (ABI). Relative mRNA levels were determined by the 2<sup>-ΔΔCt</sup> method and normalized to β-actin. The control group's average was set as 1, and all results were presented as relative mRNA expression. Sequences of the primers were listed in Table 1.

### RNA-sequencing and bioinformatics analysis

Total RNA was extracted from adipose tissues. The samples were then sequenced using Illumina NovaSeq 6000 (PE150, from Berry Genomics). After pre-mapping sequencing quality evaluation by FastQC (version: 0.10.1), the reads were mapped to the mouse reference genome (genome version: mm10) with hisat2 (version: 2.1.0) to get uniquely mapped reads using default parameters. Htseq-count from HTSeq (version: 0.9.1) was used to calculate the gene count matrix, and StringTie (version: 1.3.3b) was used to calculate gene expression values (FPKM). Differential gene expression (DGE) was analyzed using the DEseq2 tool (version: 1.18.1). The genes with low expression across all samples (FPKM < 0.5 in all samples) were removed, adjusted *P*-value below 0.05 was considered significant.

### Mitochondrial number detection with qPCR

To quantify mitochondrial number, we utilized qPCR to measure the relative amount of mitochondrial DNA (mtDNA) in samples (16). DNA was extracted from tissues or cells using a DNA extraction kit (DC102, Vazyme, China). The qPCR reactions were performed using specific primers for the mitochondrial cytochrome c oxidase subunit I (*Co1*) gene of the mtDNA and the nuclear DNA (nDNA), Ubiquinone

TABLE 1.

Name	5'→3'
<i>Atp5e</i> F	CAGGCTGGACTCAGCTACATC
<i>Atp5e</i> R	GTTTCGCTTTGAACCTCGGTCTT
<i>Atp5g2</i> F	CAGTGGAGTTGAAGCGACCA
<i>Atp5g2</i> R	TGTCGATGTCCCTTGAAATGG
<i>Atp5g3</i> F	GTAGGAGTTGTGTTCTGGTG
<i>Atp5g3</i> R	GCTTCAGACAAGGCAAAATCCAG
<i>Atp5k</i> F	GGAGAGGAGAATAGCAGCGG
<i>Atp5k</i> R	ATCTTGAGCTTCCGCCAGTT
<i>Atp5o</i> F	TCTCGACAGGTTCCGAGCTT
<i>Atp5o</i> R	AGAGTACAGGGCGGTTGCATA
<i>Cebpb</i> F	CAACCTGGAGACGCAGCACAAG
<i>Cebpb</i> R	GCTTGAACAAGTTCGCCAGGGT
<i>Cidea</i> F	TGCTCTTCTGTATCGCCAGT
<i>Cidea</i> R	GCCGTGTTAAGGAATCTGCTG
<i>Cox4i1</i> F	ATTGGCAAGAGAGCCATTTCTAC
<i>Cox4i1</i> R	CACGCCGATCAGCGTAAGT
<i>Cox4i2</i> F	ACAGTGATGGGCTCGCTTCTT
<i>Cox4i2</i> R	CTGTGGGCTTTCGGTTCCTCC
<i>Cox5a</i> F	GCCGCTGTCTGTTCCATTC
<i>Cox5a</i> R	GCATCAATGTCTGGCTTGTGAA
<i>Cox6b1</i> F	GAACTGTTGGCAGAACAACCTGG
<i>Cox6b1</i> R	ATGACAGGGACAGAGGCACTT
<i>Cox6c</i> F	GCGTCTGCGGGTTCATATTG
<i>Cox6c</i> R	TCTGCATACGCCCTTCTTCTTG
<i>Cox7c</i> F	ATGTTGGCCAGAGTATCCG
<i>Cox7c</i> R	ACCCAGATCCAAAGTACACGG
<i>Cox8b</i> F	TGTGGGGATCTCAGCCATAGT
<i>Cox8b</i> R	AGTGGGCTAAGACCCATCCTG
<i>Dgat1</i> F	TCCGTCAGGGTGGTAGTG
<i>Dgat1</i> R	TGAACAAAGAATCTTGACAGCA
<i>Ndufa1</i> F	ATGTGGTTCGAGATTCTCCCT
<i>Ndufa1</i> R	TGGTACTGAACACGAGCAACT
<i>Ndufa11</i> F	CCTGTTCAAGATCGGCAAGC
<i>Ndufa11</i> R	CCATCTCATGCAGCAAGCCT
<i>Ndufa2</i> F	CGCTGTACAGTGTCCCTTCA
<i>Ndufa2</i> R	CAGTGTGCGCAGTAAGAGG
<i>Ndufa3</i> F	GGCCACACCCTACAACACTAC
<i>Ndufa3</i> R	CAGGCATGTTCCCGTCTATCT
<i>Ndufa4</i> F	AGCAGCACTGTATGTGATGCGC
<i>Ndufa4</i> R	TGTAGTCCACATTCACAGAGTAGA
<i>Ndufb10</i> F	CAGCATGCCAAGAACCAGAC
<i>Ndufb10</i> R	TGTGATGCTTGGCAGCTCGAC
<i>Ndufb5</i> F	GACGACAAACAGTCTCTTGCC
<i>Ndufb5</i> R	CGAAGACTGTCGCTCCTGT
<i>Ndufs7</i> F	TGCGCAGAGTTTCATCAGAGT
<i>Ndufs7</i> R	ATGAGAGAGCTTGGGGACCA
<i>Npr3</i> F	GGGGTCCACGAGGTTTTTC
<i>Npr3</i> R	CTCCACGAGCCATCTCCGTA
<i>Pgc1a</i> F	AATGAGGGCAATCCGCTTTCA
<i>Pgc1a</i> R	GAAAGTGGTGTAGCGACCAATC
<i>Ucp1</i> F	AGGCTTCCAGTACCATTAGGT
<i>Ucp1</i> R	CTGAGTGAGGCAAAGCTGATTT
<i>Uqcrl0</i> F	ATCCCTTCGCGCTGACT
<i>Uqcrl0</i> R	GTGCTCGTAGATCGCGTCT
<i>Uqcrb</i> F	CCATAAGAAGGCTTCTGAGGAC
<i>Uqcrb</i> R	TTTGTCCACTGATCCTTAGGCAA
<i>Uqcrl1</i> F	GTGGACCCCTACAACAGTG
<i>Uqcrl1</i> R	CGGGAAGACACCGGATTATCA
<i>Uqcrl2</i> F	CCTACAGCTTGTCCGCTTT
<i>Uqcrl2</i> R	GATCAGGTAGACCCTAAAACG
<i>β-actin</i> F	GTCAGTTGACATCCGTAAAGA
<i>β-actin</i> R	GCCGGACTCATCGTACTCC
<i>Co1</i> F	TGCTAGCCGCAGGCATTAC
<i>Co1</i> R	GGGTGCCAAAGAATCAGAAC
<i>Ndufv1</i> F	CTTCCCCTGGCCTCAAG
<i>Ndufv1</i> R	CCAAAACCCAGTGATCCAGC

Oxidoreductase Core Subunit VI (*Ndufv1*) gene as a reference. The primer sequences were as reported by Guo *et al.* (2009) (16) and were presented in Table 1. The relative mtDNA content was calculated using the 2<sup>-ΔΔCt</sup> method,



normalizing the Ct values of the *Col* gene to the Ct values of the *Ndufo1* gene.

### Western blot

For Western blot analysis, tissues or cells were lysed in RIPA buffer, containing phosphatase inhibitor and protease inhibitor. Protein samples (20–50 µg) were separated using 10% SDS-PAGE gel and then transferred onto a polyvinylidene fluoride membrane (0.22 µm, Millipore). The membranes were blocked with 5% fat-free milk and then incubated with primary antibodies: anti-UCPI (Abcam, ab10983, 1:1000), anti-NPR-C (Abcam, ab97389, 1:1000), anti-NPR-B (Abclonal, A19255, 1:1000), anti-PGC-1 $\alpha$  (Abclonal, A19674, 1:1000), anti-OxPhos Cocktail (Invitrogen, 45–8099, 1:1000), anti-p-P38 (CST, 4511S, 1:1000), anti-P38 (CST, 8690S, 1:1000), anti-p-AKT (CST, 4060S, 1:1000), anti-AKT (CST, 4691S, 1:1000), anti- $\alpha$ -tubulin (Proteintech, HRP-66031, 1:10,000). Membranes were incubated with primary antibodies overnight at 4°C. Using TBST to wash membranes and incubating with HRP conjugated secondary antibody for 1 h at room temperature. After incubation with a chemiluminescent reagent (Tanon, 180–5001), the bands were quantified using Quantity One imaging software (BioRad Laboratory, Spain).

### NAD/NADH measurement

NADH levels were measured using the NADH Assay Kit (Abcam, ab65348) according to the manufacturer's instructions. Briefly, 20 mg of adipose tissue was homogenized with extraction buffer. After centrifugation, the supernatants were used to measure total NAD and NADH (NADt). Aliquots of 200 µl supernatant were heated at 60°C for 30 min to measure NADH.  $\text{NAD/NADH ratio} = (\text{NADt} - \text{NADH})/\text{NADH}$ .

### ATP measurement

Adipose ATP levels were measured using the ATP Content Assay Kit (Solarbio, BC0300). Briefly, 0.1 g of adipose tissue was homogenized in 1 ml extraction liquid, followed by centrifugation at 4°C for 10 min. The supernatants were mixed thoroughly with chloroform. After 3 min incubation, ATP was immediately measured by recording the light absorption at 340 nm.

### Oxygen consumption rate (OCR) measurements

SVF cells were plated in a Seahorse 96-well microplate at  $1 \times 10^4$  cells per well. SVF cells were differentiated into white adipocytes and infected with sh*Npr3* or sh*Npr2* for 48 h. OCR was measured using the Seahorse XFe96 Analyzer (Seahorse Bioscience). Cellular respiration was quantified at baseline and in response to 1 µM oligomycin, 2 µM carbonylcyanide-4-(trifluoromethoxy) phenylhydrazone (FCCP), and 0.5 µM antimycin A/rotenone. The following parameters were calculated: Basal Respiration: Last rate measurement before the first injection minus the non-mitochondrial respiration rate. ATP Production: Last rate measurement before oligomycin injection minus the minimum rate measurement after oligomycin injection. Maximal Respiration: Maximum rate measurement after FCCP injection minus the non-mitochondrial respiration rate. Spare Respiratory Capacity: Maximal respiration minus basal respiration.

### Transmission electron microscopy (TEM)

SVF-induced white adipocytes were fixed with 2.5% glutaraldehyde buffer for 1 h at room temperature. The cells were then gently scraped down and centrifuged at 4°C for 5 min. Cell pellets were embedded and cut into 70-nm sections. Sections were observed using a JEM-1400 transmission electron microscope (JEOL, Japan).

### Lipid level measurement

Serum levels of non-esterified fatty acids (NEFA) were measured using the NEFA determination kit (Nanjing Jiancheng Bioengineering Institute, A042-2-1) according to the manufacturer's instructions. Serum levels of triglycerides (TG), cholesterol (CHO), high-density lipoprotein (HDL), and low-density lipoprotein (LDL) were measured using an Auto Chemistry Analyzer (Rayto Life and Analytical Science, Chemray 800). TG levels in the liver were measured using a Triglyceride Assay Kit (Nanjing Jiancheng Bioengineering Institute, A110-1-1). Liver tissue (0.1 g) was weighed and homogenized in PBS at a ratio of 1 g of tissue to 9 ml of PBS. The homogenate was centrifuged at 2500 rpm for 10 min at 4°C. The supernatant was collected for measurement, and the results were normalized to liver protein levels.

### Measurement of cAMP, cGMP, and calcium levels

Intracellular cAMP and cGMP levels were measured using the Cyclic adenosine monophosphate (cAMP) ELISA Kit (Elabscience, E-EL-0056), and the Cyclic guanosine monophosphate (cGMP) ELISA Kit (Elabscience, E-EL-0083), respectively, according to the manufacturer's instructions. Calcium levels were measured using the Calcium Assay Kit (Beyotime, S1063S) following the manufacturer's instructions.

### Statistics

Data are expressed as mean  $\pm$  SEM. GraphPad Prism (v10.2.0; GraphPad Software) was used for all statistical analyses. The normal distribution of the data was verified using the Shapiro-Wilke test. For comparisons between two datasets, a two-tailed, unpaired Student's *t*-test was conducted. One-way ANOVA followed by Tukey's test was used for comparing three or more groups. Corrections for multiple comparisons were made in the figure legends, and *P*-values were reported with the following significance levels: ns, not significant;  $P \geq 0.05$ ; \* $P < 0.05$ ; \*\* $P < 0.01$ ; \*\*\* $P < 0.001$ .

## RESULTS

### Cold-induced decrease of NPR-C expression in eWAT

SWAT is located below the dermis and above the fascia, serving as an energy storage depot and contributing to heat preservation (17). While eWAT, predominantly visceral adipose tissue, surrounds the epididymis of mice protecting the epididymal and other abdominal organs. An accumulation of eWAT poses considerable health risks, including diabetes and nonalcoholic fatty liver disease (18). Therefore, improvement of eWAT metabolic dysfunction is a therapeutic strategy to combat these metabolic disorders.

To further elucidate the molecular drivers of eWAT energy metabolism, we analyzed gene expression profiles from the public Gene Expression Omnibus (GEO) database. It has been reported that cold exposure (19) and dietary restriction (DR) (20) activate AT browning and thermogenesis, while a high-fat diet inhibits thermogenesis (21). *Npr3* mRNA expression was down-regulated after being subjected to 12 weeks of DR compared to those on an ad-libitum diet (AL) in eWAT of mice, as indicated by data from the GSE27213 dataset. Similarly, *Npr3* mRNA expression was reduced in an in vitro cold exposure model, where white adipocytes were maintained at 31°C compared to 37°C (GSE159451). Conversely, in an eight-week high-fat diet (HFD) model (GSE167311), *Npr3* mRNA expression was significantly up-regulated in eWAT compared to normal chow diet (NCD) conditions (Fig. 1A). To further validate our observations, we assessed *Npr3* mRNA expression in response to different temperature exposures (4°C, -10°C, and -20°C) in a cold exposure model (GSE74062). Our analysis demonstrated a temperature-dependent decrease in *Npr3* mRNA expression within eWAT (Fig. 1B). These findings strongly implement the pivotal role of NPR-C in regulating eWAT metabolism, particularly in browning and thermogenesis. Next, a comparative analysis of NPR-C expression between eWAT and sWAT revealed significantly higher levels of both mRNA and protein in eWAT (Fig. 1C, D). Consistent with the findings from the GSE159451, we confirmed that *Npr3* mRNA levels showed a significant decrease after 72 h of cold exposure (Fig. 1E). In accordance with previous studies, we also observed increased UCPI expression in WAT after cold exposure (Fig. 1G, I). Furthermore, we observed a reduction in NPR-C protein levels in both sWAT and eWAT following cold exposure, as evidenced by Western blot and immunofluorescence staining (Fig. 1F–I). These results suggest that the decreased expression of NPR-C may be associated with cold-induced thermogenic response.

### NPR-C deficiency promotes adipose tissue thermogenesis

Next, we employed WT and *Npr3* KO (KO) mice to investigate the impact of NPR-C in adipose metabolism (22). Notably, akin to previously reported findings, (23) KO mice had a markedly elongated body shape and reduced body weight compared to WT mice (Fig. 2A). Furthermore, KO mice displayed smaller eWAT, sWAT, and brown adipose tissue (BAT) (Fig. 2B). Nevertheless, there were no significant changes in the weights of the kidneys, lungs, hearts, and livers between the two groups (Fig. 2B). H&E staining revealed smaller lipid droplets and adipocytes in the eWAT and sWAT of KO mice (Fig. 2C, D). Since eWAT exhibited the most pronounced histopathological changes, which correlated with higher NPR-C expression levels (Fig. 1C, D), our subsequent studies focused primarily on eWAT. The knockout of *Npr3* led to the up-regulation of

browning-related genes, such as *Ucp1*, *Pgc1α*, and cell-death-inducing DNA fragmentation factor- $\alpha$ -like effector A (*Cidea*) (Fig. 2E), which are key regulators of brown adipose cell function (24). Additionally, thermogenesis-related genes (*Cox4i2*, *Ndufa4*, *Cebpb*, *Elavl3*) and lipogenesis-related genes (*Dgat1*, *Fasn*) were also up-regulated in the eWAT of KO mice compared to WT mice (Fig. 2E). Meanwhile, the inflammatory factor tumor necrosis factor  $\alpha$  (Tnf $\alpha$ ) was decreased, and the angiogenesis gene *Cd31* was increased in KO mice (Fig. 2E). Moreover, Western blot and immunofluorescence staining confirmed the increased expression of UCPI in eWAT (Fig. 2F, G). In conclusion, our study demonstrates that the loss of NPR-C augments browning and thermogenic gene expression reduces inflammation in eWAT. These findings highlight the crucial regulatory role of NPR-C in WAT biology.

### NPR-C deficiency leads to enhanced mitochondrial function in cold exposure

To gain deeper insights into the role of NPR-C in adipose browning and thermogenesis, we subjected both WT and KO mice to cold exposure. The cold-induced morphological changes, characterized by smaller adipocytes, were more pronounced in KO mice, particularly in eWAT, but to a lesser extent in sWAT (Fig. 3A, B). We conducted RNA-sequencing analysis using eWAT samples from WT and KO mice after cold exposure to explore the underlying mechanisms. RNA-sequencing analysis identified 269 genes significantly up-regulated, and 372 genes significantly down-regulated in KO mice ( $|\log_2\text{FoldChange}| > 1$ ,  $P < 0.05$ ) compared to WT mice (Fig. 3C). Kyoto Encyclopedia of Genes and Genomes (KEGG) enrichment analysis of the differentially expressed genes revealed that NPR-C ablation impacted multiple cellular activities and signaling pathways including oxidative phosphorylation and thermogenesis (Fig. 3D). Gene Ontology (GO) enrichment highlighted a significant association with mitochondrial activity, such as mitochondrion, mitochondrial part, and mitochondrial protein complex in KO mice (Fig. 3E). Heatmap analysis further confirmed the elevated expression of genes related to mitochondrial respiratory chain complexes (Fig. 3F). qPCR confirmed the up-regulation of genes related to mitochondrial respiratory chain complexes in KO mice, including those involved in complex I (NADH-Q oxidoreductase), complex III (UQ-cytochrome C oxidase), complex IV (cytochrome C oxidase), and complex V (ATP synthase) (Fig. 3G). The levels of complex II (succinate dehydrogenase) and complex III proteins exhibited significant increases in KO mice (Fig. 3H). The mitochondrial respiratory chain complexes operate via a series of redox processes to produce ATP, providing essential energy for body tissues. To assess the impact of NPR-C deficiency on mitochondrial function, we quantified the NAD/

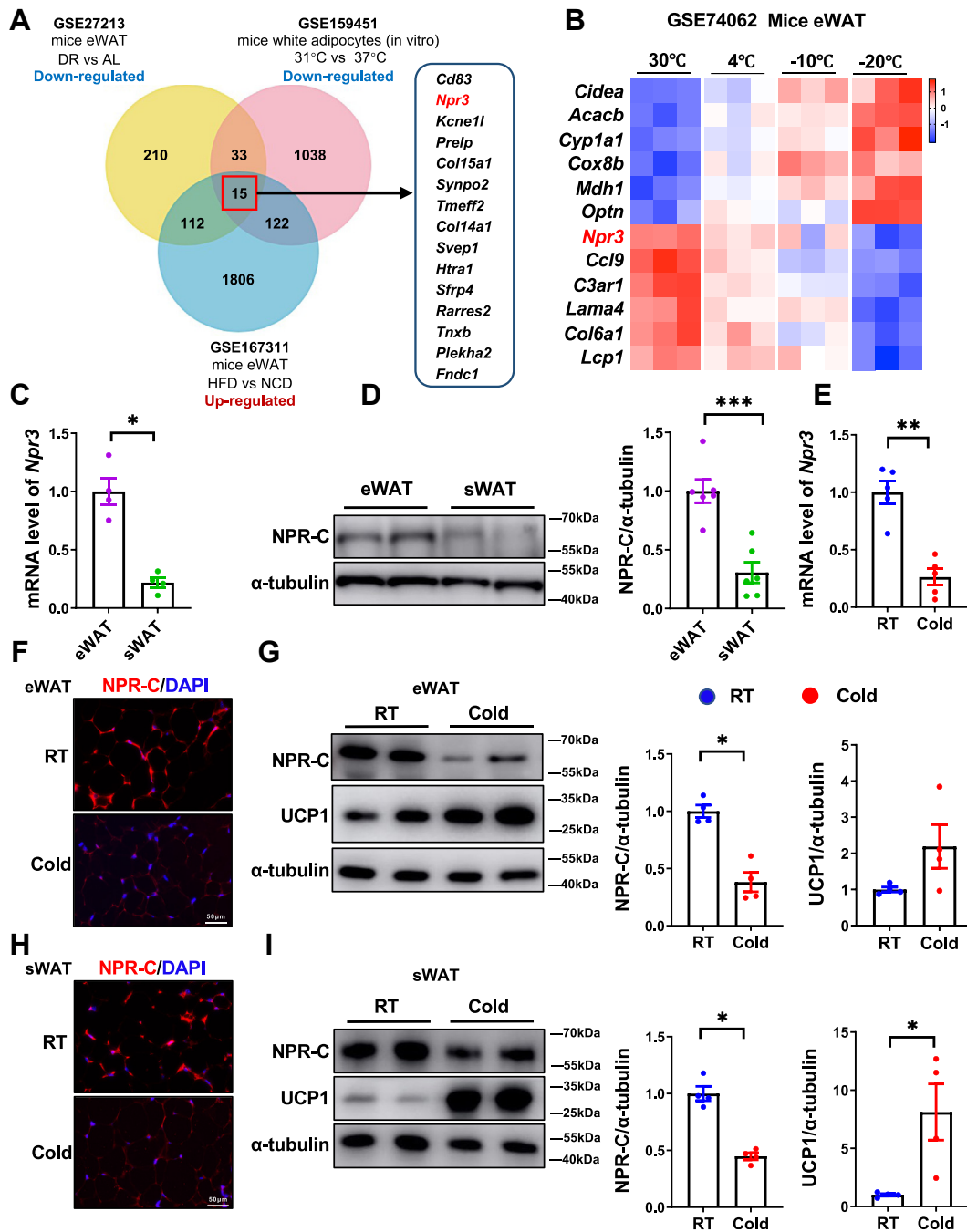


**Fig. 1.** Cold-induced decrease of NPR-C expression in epididymal WAT (eWAT). **A:** Venn diagram identifying candidate genes for WAT metabolic disorders. **B:** Heatmap of differential gene expression from mice eWAT exposed to different temperatures. **C:** Relative mRNA expression of *Npr3* in mice eWAT and subcutaneous WAT (sWAT). **D:** Western blot analysis and quantification data of NPR-C in mice eWAT and sWAT. **E** through **I.** WT male mice were individually housed at room temperature (RT) or 4°C (Cold) for 72 h. **E:** qPCR analysis of *Npr3* mRNA in eWAT of mice from RT and Cold. **F:** Representative images of NPR-C (red) immunofluorescence in eWAT from RT and Cold. DAPI was used to stain the nucleus in blue. **G:** Western blot analysis and quantification data of NPR-C and uncoupling protein I (UCP1) protein expression in eWAT from RT and Cold. **H:** Representative images of NPR-C (red) immunofluorescence in sWAT from RT and Cold. DAPI was used to stain the nucleus in blue. **I:** Western blot analysis and quantification data of NPR-C and UCP1 protein expression in sWAT from RT and Cold. Data are presented as mean  $\pm$  SEM. Data were analyzed by unpaired Student's *t*-test. \**P* < 0.05, \*\**P* < 0.01, \*\*\**P* < 0.001.

NADH ratio and ATP levels in fresh eWAT tissues from WT and KO mice. The data revealed significant elevations in NAD/NADH ratios and ATP levels in KO mice (Fig. 3I, J). Next, we quantified the number of mitochondria in eWAT from both groups by

measuring the mitochondrial DNA content (16, 25). The results demonstrated that the mitochondrial numbers in the eWAT of KO mice were significantly increased compared to WT mice (Fig. 3K). These findings collectively suggest that NPR-C plays a

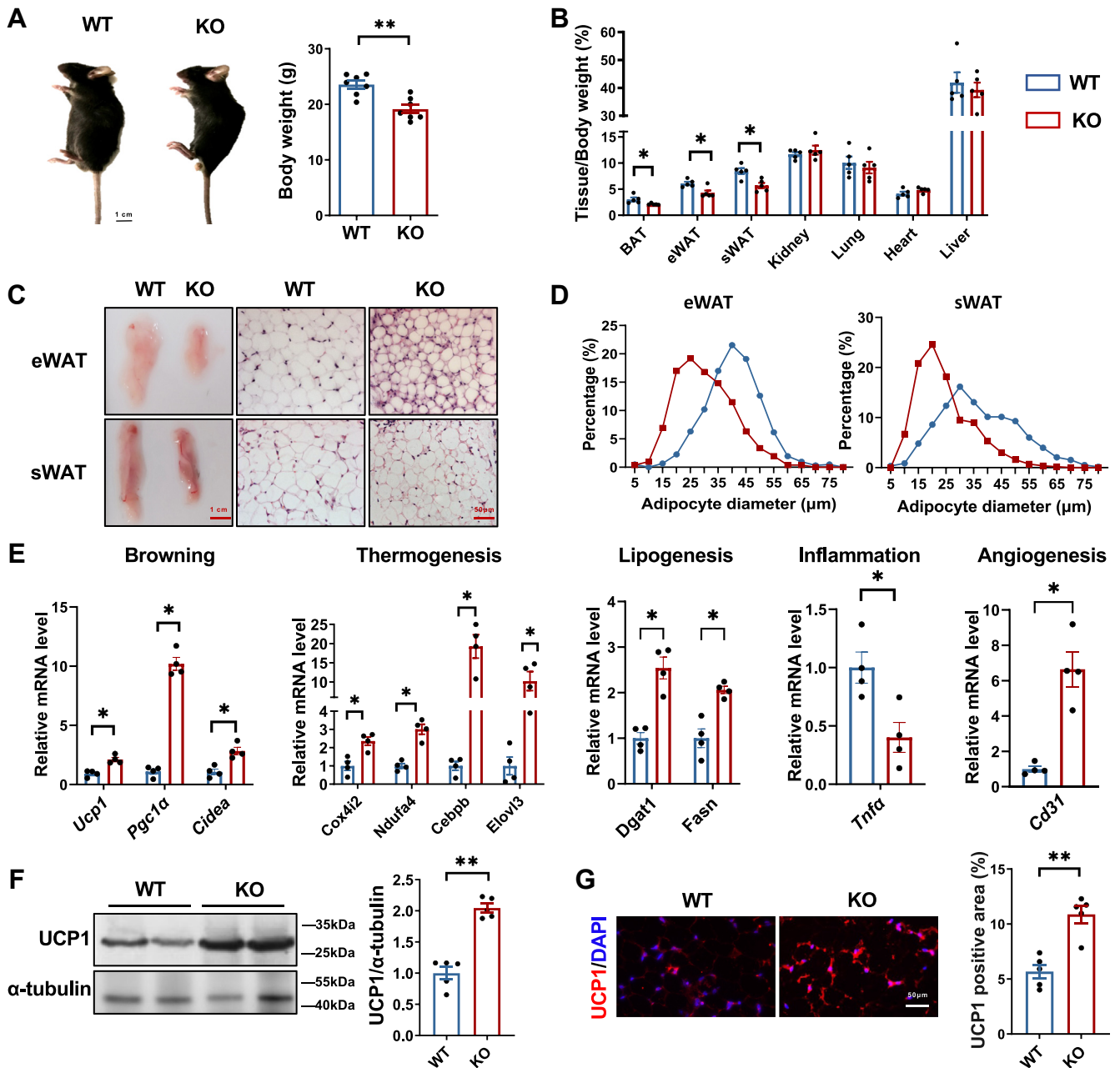


**Fig. 2.** NPR-C deficiency promotes adipose tissue thermogenesis. **A:** Representative images and body weight of WT and *Npr3* knockout (KO) mice. **B:** Tissue weight of WT and KO mice. **C:** Representative images and H&E staining of eWAT and sWAT of WT and KO mice. **D:** Distribution of adipocyte size in eWAT (left) and sWAT (right) of WT and KO mice. The percentage of cells in relation to cell diameter for WT and KO mice (WT,  $n = 5$ ; KO,  $n = 5$ . Five H&E-stained slides per mouse). **E:** qPCR analysis of browning, thermogenesis, lipogenesis, inflammation, and angiogenesis genes expression in eWAT from WT and KO mice. **F:** Western blot analysis and quantification data of UCP1 protein expression in eWAT from WT and KO mice. **G:** Representative images and quantification data of UCP1 (red) immunofluorescence in eWAT from WT and KO mice. DAPI was used to stain the nucleus in blue. Data are presented as mean  $\pm$  SEM. Data were analyzed by unpaired Student's *t*-test. \* $P < 0.05$ , \*\* $P < 0.01$ .

pivotal role in regulating mitochondrial biogenesis and function in adipose tissues.

### NPR-C deficiency attenuates HF/HS-induced metabolic dysfunction

WAT disorders have a significant impact on the pathophysiology of metabolic disorders by regulating various metabolic processes and systemic energy balance (26). Therefore, we investigated whether NPR-C

plays a regulatory role in the development of metabolic diseases. We utilized a model of a Western diet, a high-fat/high-sugar (HF/HS) diet, which is commonly used to mimic the components of fast food (27). Interestingly, KO mice exhibited less weight gain compared to WT mice (Fig. 4A, B), indicating an innate resistance to diet-induced obesity in KO mice. We noted a marked decrease in the weights of the sWAT, eWAT, and kidney in KO mice (Fig. 4C). These observations were



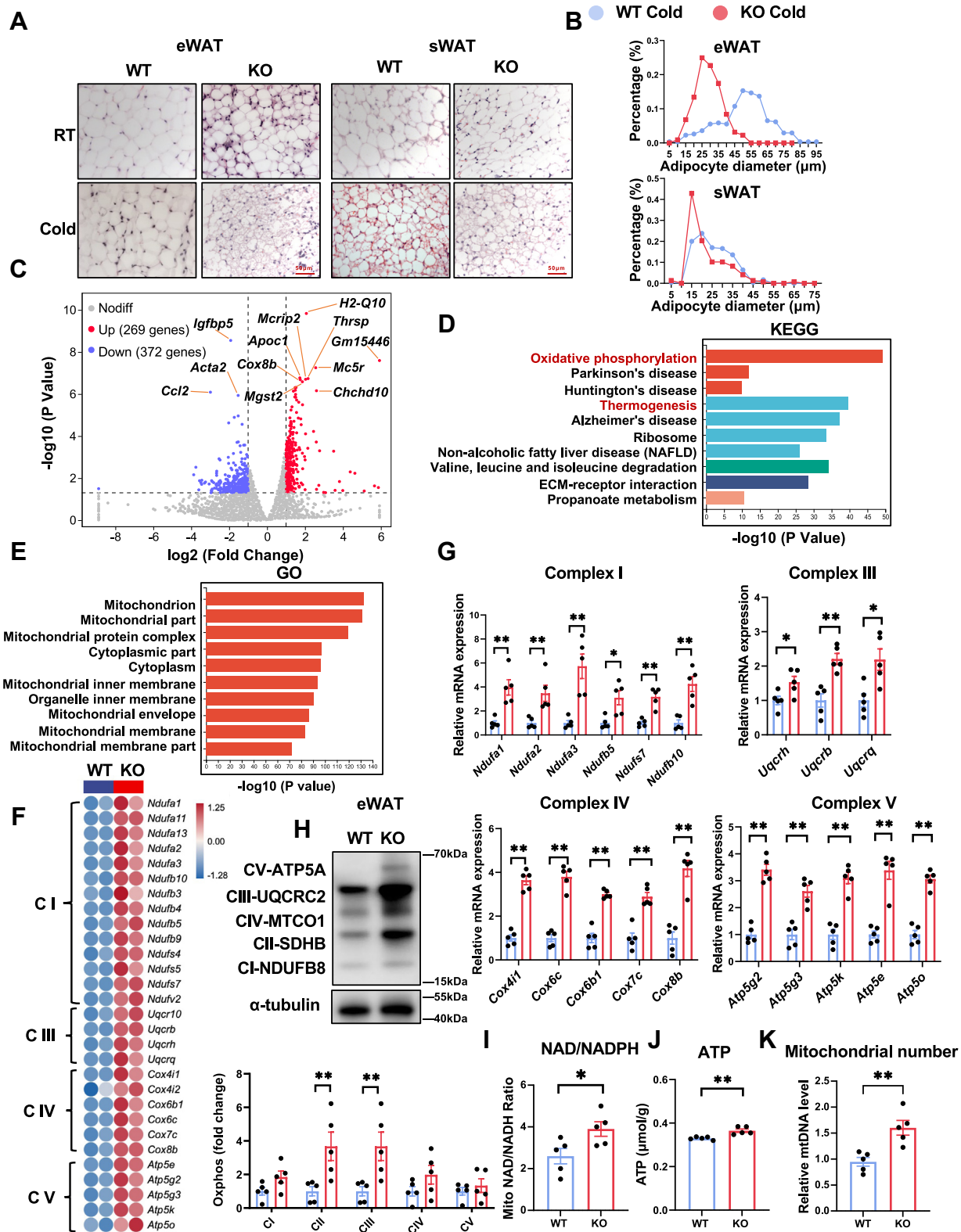


**Fig. 3.** NPR-C deficiency leads to enhanced mitochondrial function in cold exposure. A: H&E staining of eWAT and sWAT from WT and KO mice exposed to RT or Cold for 72 h. B: Distribution of adipocyte size in eWAT (top) and sWAT (bottom). (WT Cold,  $n = 5$ ; KO Cold,  $n = 5$ . Five H&E-stained slides per mouse). C: Volcano plot comparisons of gene expression in eWAT. D: Top KEGG terms in eWAT. E: Top GO terms in eWAT. F: Heatmap of up-regulated genes related to mitochondrial respiratory chain complexes in eWAT. G: qPCR analysis of mitochondrial respiratory chain complexes in eWAT. CI: complex I; CII: complex II; CIII: Complex III; CIV: complex IV; CV: complex V. H: Western blot analysis and quantification data of mitochondrial respiratory chain complex protein expression in eWAT. I: NAD/NADH ratio in eWAT. J: ATP levels in eWAT. K: Relative mtDNA levels in eWAT. Data are presented as mean  $\pm$  SEM. Data were analyzed by unpaired Student's  $t$ -test. \* $P < 0.05$ , \*\* $P < 0.01$ .



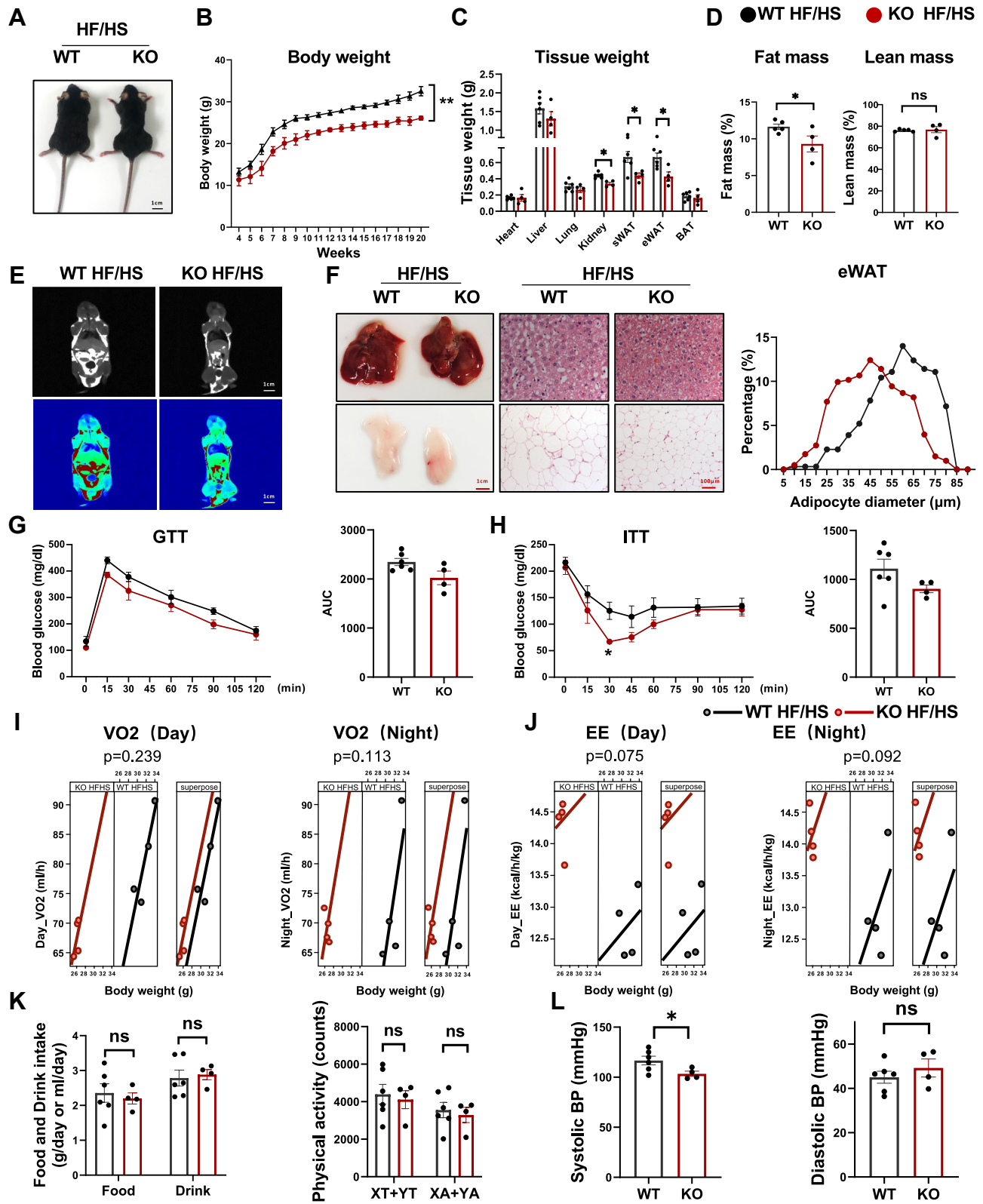


**Fig. 4.** NPR-C deficiency attenuates high-fat/high-sugar (HF/HS)-induced metabolic dysfunction. The HF/HS diet started from 4 weeks and lasted for 14 weeks. **A:** Representative images of 14-week-old male WT and KO mice. **B:** Body weight curve of WT and KO mice induced by HF/HS diet. **C:** Tissue weight of WT and KO mice induced by HF/HS diet. **D:** Fat mass and lean mass of WT-HF/HS and KO-HF/HS mice. **E:** Representative fat highlighting images (top, fat is white), highlighted pseudo-color image (bottom, fat is red) in magnetic resonance imaging (MRI) analysis. **F:** Representative images and H&E staining of liver and eWAT, and distribution of adipocyte size in eWAT (WT,  $n = 4$ ; KO,  $n = 4$ . Five H&E-stained slides per mouse) in WT-HF/HS and KO-HF/HS mice. **G:** Glucose tolerance test (GTT) (left) and calculated area under the curve (AUC) (right) in WT-HF/HS and KO-HF/HS mice. **H:** Insulin tolerance test (ITT) (left) and calculated AUC (right) in WT-HF/HS and KO-HF/HS mice. **I:** ANCOVA analysis results of  $O_2$

further supported by a decrease in body fat mass and no significant difference in lean mass between KO and WT mice (Fig. 4D). MRI analysis clearly displayed the distribution of adipose tissues and revealed a significant reduction of adipose deposition in KO mice (Fig. 4E). Histological staining confirmed that KO mice displayed smaller lipid droplets in eWAT (Fig. 4F). Furthermore, loss function of NPR-C tended to ameliorate the lipid accumulation induced by the HF/HS diet in liver (Fig. 4C, F). In GTT and ITT measurements, KO mice exhibited a trend toward improved insulin sensitivity (Fig. 4G, H). Metabolic cage experiments were conducted to investigate metabolic parameters in the two groups of mice. Notably, under the HF/HS diet, KO mice showed an increasing trend in nighttime oxygen consumption and both daytime and nighttime energy expenditure, suggesting that KO mice may have higher energy expenditure than WT mice (Fig. 4I, J) without notable differences in energy intake or physical activity (Fig. 4K). Consistent with previous studies, (22) KO mice displayed lower systolic blood pressure, with no significant difference in diastolic blood pressure (Fig. 4L). Collectively, our findings demonstrate that NPR-C deficiency can ameliorate diet-induced obesity and metabolic dysfunction.

### The impact of NPR-C on mitochondrial function in vitro

To determine the mechanism responsible for NPR-C's impact on mitochondrial function, we utilized *Npr3* shRNA to knock down *Npr3* expression both in mRNA and protein levels (Fig. 5A, B). It was essential to assess whether *Npr3* knockdown affected the efficiency of adipocyte differentiation in SVF cells. Following *Npr3* knockdown, SVF cells were induced to differentiate into white adipocytes. Oil Red O staining revealed that *Npr3* knockdown did not impact the adipogenic efficiency of SVF cells (Fig. 5C). Subsequent qPCR analysis indicated that *Npr3* knockdown led to an up-regulation of *Ucp1* mRNA expression (Fig. 5D). Furthermore, we observed the mitochondrial respiratory chain complexes had an up-regulation in both mRNA and protein levels in *Npr3* knockdown adipocytes (Fig. 5E, F). Next, we explored the effect of *Npr3* knockdown on mitochondrial number and morphology in vitro. Transmission electron microscopy (TEM) analysis showed that although a slight increase in mitochondrial count was observed in *Npr3* knockdown adipocytes, their size remained constant. Notably, mitochondria exhibited clustering near the nucleus rather than a uniform distribution. Moreover, mitochondrial electron density was higher in the sh*Npr3*

group (Fig. 5G), suggesting potential alterations in mitochondrial structure or function (28). An increase in mtDNA levels in the *Npr3* knockdown group was also observed (Fig. 5H), indicating enhanced mitochondrial biogenesis.

Previous studies have shown that CL316,243, a highly selective and potent  $\beta_3$ -adrenergic receptor agonist, elevates thermogenesis and metabolic rate in adipose tissue by specifically activating UCP1, thereby promoting adipose browning (29). Similar to CL316,243 stimulation, *Npr3* knockdown elevated protein levels of PGC1 $\alpha$  and UCP1 (Fig. 5I). Our findings suggest that NPR-C plays a regulatory role in mitochondrial energy metabolism, with its loss of function mimicking the effects of  $\beta_3$ -adrenergic receptor activation by CL316,243. These findings highlight the potential of targeting NPR-C for metabolic interventions aimed at enhancing mitochondrial function and energy expenditure.

### NPR-C regulates mitochondrial function dependent on NPR-B

To determine the signaling pathways through which NPR-C affects mitochondrial energy homeostasis, KEGG analysis of RNA-sequencing data identified noteworthy up-regulation of the PI3K/AKT, peroxisome proliferator-activated receptor (PPAR), and AMP-activated protein kinase (AMPK) pathways in KO mice when compared to WT mice (Fig. 6A). Western blot analysis confirmed that both *Npr3* knockdown and CL316,243 stimulation increased the phosphorylation of AKT and p38 in a short time (Fig. 6B). It is reported that the activation of both AKT and p38 promotes thermogenesis (30–32). The up-regulation of UCP1 protein caused by *Npr3* knockdown, was reversed by the inhibition of AKT with MK2206 and p38 with SB203580 (Fig. 6C, D) (6). Since CNP mediates metabolic functions by interacting with both NPR-B and NPR-C, (8) we further examined whether NPR-B signaling is involved in mitochondrial function following *Npr3* knockdown. Surprisingly, the up-regulated protein levels of PGC1 $\alpha$  and UCP1 induced by *Npr3* knockdown were reversed by additional knockdown of *Npr2* (Fig. 6E). Consistently, the phosphorylation of AKT and p38 was diminished in the same group (Fig. 6E). Furthermore, comprehensive oxygen consumption analysis revealed that a decline in *Npr2* expression restores the increase in basal respiration and tends to restore the increase in ATP coupling, and maximum respiration rate caused by *Npr3* knockdown (Fig. 6F).

In adipocytes, cAMP, cGMP, and calcium signaling are integral for proper adipose function, and these

consumption (VO<sub>2</sub>) of WT-HF/HS and KO-HF/HS mice over 48 h. *P* value was between two groups. J: ANCOVA analysis results of energy expenditure (EE) of WT-HF/HS and KO-HF/HS mice over 48h. *P* value was between two groups. K: Food and drink intake (left) and physical activity (right) of WT-HF/HS and KO-HF/HS mice. L: Systolic (left) and diastolic (right) blood pressure (BP) of WT-HF/HS and KO-HF/HS mice. Data are presented as mean  $\pm$  SEM. Data were analyzed by unpaired Student's *t*-test. \**P* < 0.05, \*\**P* < 0.01, ns: not significant.

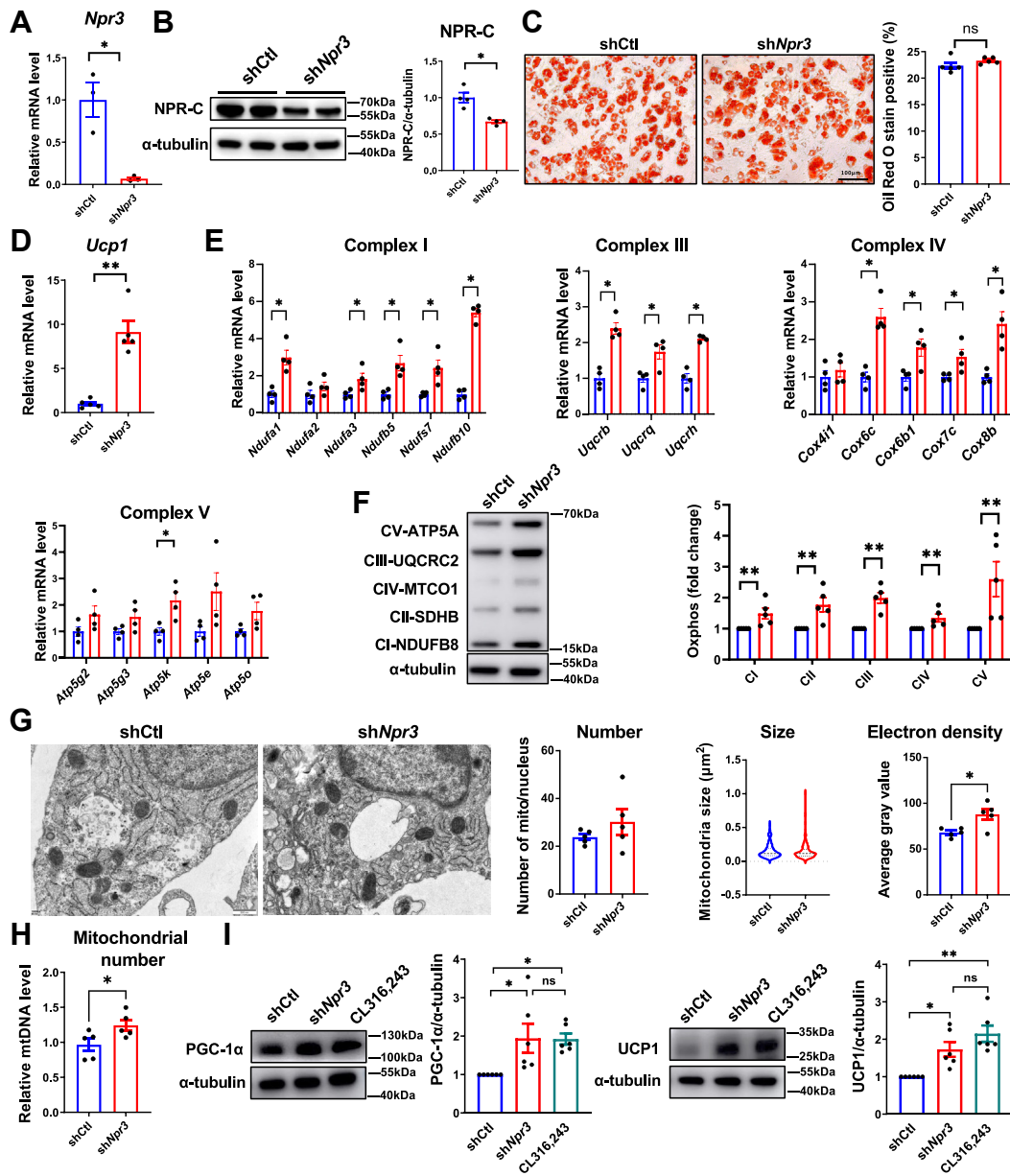


**Fig. 5.** The effect of NPR-C on mitochondrial function in vitro. **A:** qPCR analysis of *Npr3* mRNA expression in SVF-induced white adipocytes transfected with scramble RNA control (shCtl) or *Npr3* shRNA (sh*Npr3*). **B:** Western blot analysis and quantification data of NPR-C protein expression. **C:** The Oil Red O staining of SVF cells transfected with shCtl or sh*Npr3* followed by induction into white adipocytes. **D:** qPCR analysis of *Ucp1* mRNA expression in SVF-induced white adipocytes transfected with shCtl or sh*Npr3*. **E:** qPCR analysis of mRNA expressions of mitochondrial respiratory chain complexes. **F:** Western blot analysis and quantification data of oxidative phosphorylation complex proteins. **G:** Transmission electron microscopy (TEM) images and analysis of SVF-induced white adipocytes transfected with shCtl or sh*Npr3*. Mitochondrial size was measured for all mitochondria in each field of view. Electron density was determined by calculating the gray value of each mitochondrion, with averages represented as single dots. **H:** qPCR analysis of the number of mitochondria. **I:** Western blot analysis and quantification data of PGC1 $\alpha$  and UCP1 protein expression in SVF-induced white adipocytes transfected with shCtl or sh*Npr3* or treated with CL316,243 for 6 h. Data are presented as mean  $\pm$  SEM. Data were analyzed by unpaired Student's *t*-test. \**P* < 0.05, \*\**P* < 0.01, ns: not significant.

pathways have been reported to be related to natriuretic peptide families (33). To elucidate the roles of NPR-C and NPR-B in adipocyte signaling, we investigated their effects on cAMP, cGMP, and calcium signaling pathways. Our results demonstrated that *Npr3* knockdown significantly increased cAMP, cGMP, and calcium levels. In contrast, the double knockdown of *Npr3* and *Npr2* showed no significant difference in

cAMP levels compared to *Npr3* knockdown alone. However, cGMP and calcium levels were significantly decreased in the double knockdown group (Fig. 6G). These findings indicate that NPR-C inhibits cGMP and calcium signaling in an NPR-B-dependent manner but inhibits cAMP signaling in an NPR-B-independent manner. These results demonstrate that NPR-C is crucial for regulating mitochondrial function via the

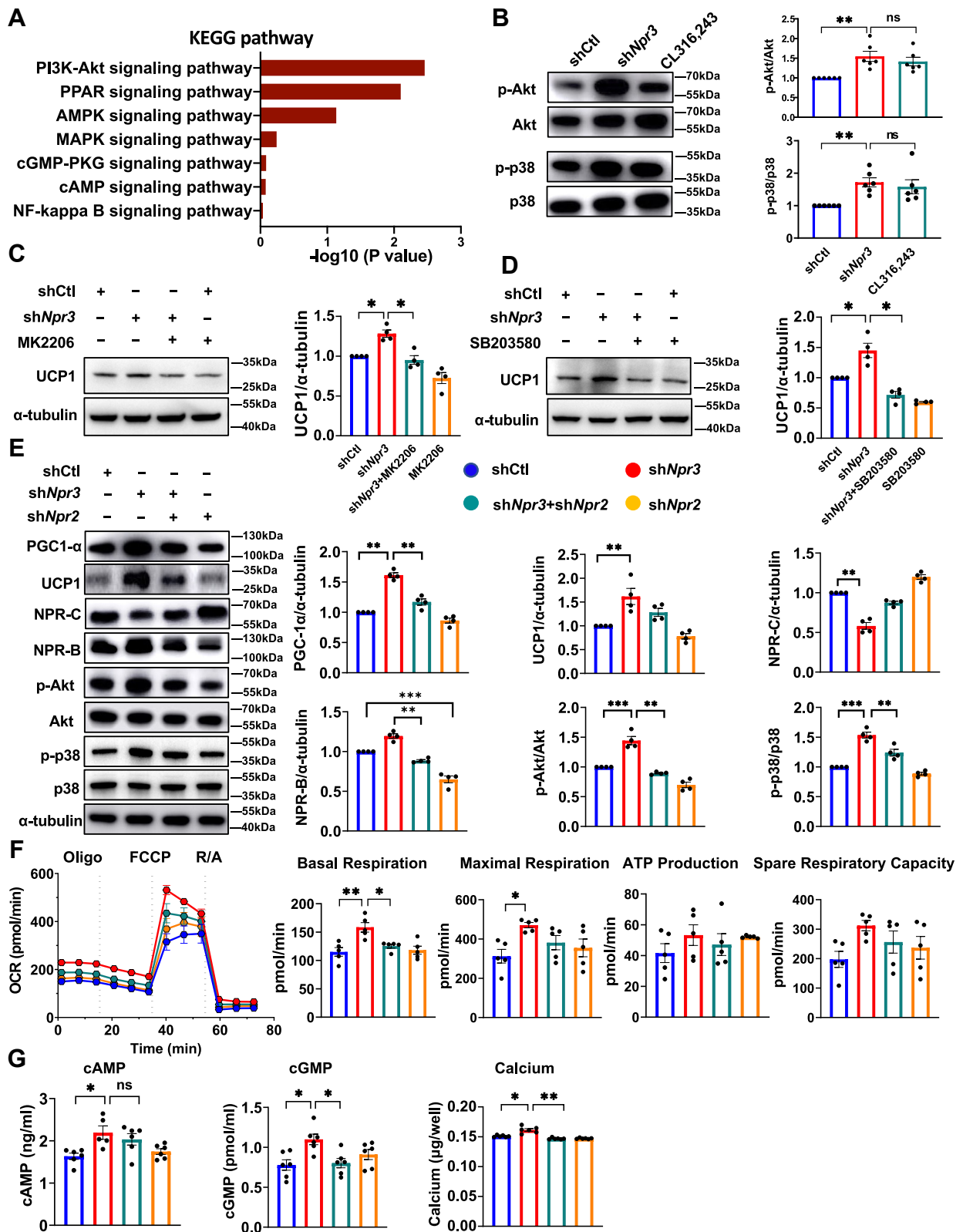


**Fig. 6.** NPR-C regulates mitochondrial function dependent on NPR-B signaling. **A:** KEGG pathways of eWAT in WT and *Npr3* KO mice in the cold-exposure model. **B:** Western blot analysis and quantification data of p-Akt/Akt and p-p38/p38 expression in SVF-induced white adipocytes transduced with shCtl or shNpr3 or treated with CL316,243 for 6 h. **C** through **D:** Western blot analysis and quantification data of UCP1 expression in SVF-induced white adipocytes transduced with shCtl or shNpr3 plus MK2206 or SB203580. **E:** Effects of shRNAs on the protein expression of PGC1 $\alpha$ , UCP1, NPR-C, NPR-B, p-Akt/Akt and p-p38/p38 in SVF-induced white adipocytes. **F:** Effects of shRNAs on oxygen consumption rate (OCR). **G:** Effects of shRNAs on cAMP, cGMP, and calcium levels. Data are presented as mean  $\pm$  SEM. Data were analyzed by one-way ANOVA followed by Tukey's test. \* $P$  < 0.05, \*\* $P$  < 0.01, \*\*\* $P$  < 0.001, ns: not significant.



AKT and p38 pathways, and this regulation is dependent on NPR-B.

### Inhibition of NPR-C mimics cold-induced adipose tissue thermogenesis

To evaluate the potential therapeutic strategy of inhibiting NPR-C for metabolic dysfunction, we initially treated SVF-induced white adipocytes with the NPR-C-specific antagonist AP-811 *in vitro*. In cultured adipocytes, AP-811 activated the p38 and AKT signaling pathways in a dose-dependent manner, similar to the effects seen with *Npr3* knockdown (Fig. 7A), suggesting that AP-811 could be an effective therapeutic agent. Next, we treated WT mice with daily injections of AP-811 for one week. Blockade of NPR-C did not affect body weight (supplemental Fig. S1A), but significantly reduced the mass of both eWAT and sWAT compared to the control group (Fig. 7B). Histological analysis showed that AP-811 induced smaller lipid droplets (Fig. 7C) without affecting lipid levels in the serum and liver (supplemental Fig. S1B, C). Additionally, AP-811 treatment up-regulated UCPI expression in both eWAT and sWAT, indicating a potential increase in energy expenditure (Fig. 7D). Moreover, AP-811 was found to increase the expression of mitochondrial respiratory chain complexes in both eWAT and sWAT, implying a potential enhancement in oxidative metabolism (Fig. 7E, F). Taken together, these results demonstrate the therapeutic potential of NPR-C in obesity and metabolic dysfunction.

## DISCUSSION

The natriuretic peptide system influences adipose tissue lipolysis, and energy expenditure, and modulates adipokine release (34, 35). In this study, our findings highlight that the deficiency of NPR-C in WAT promotes mitochondrial function and attenuates diet-induced obesity (Fig. 8). Specifically, NPR-C exhibited higher expression levels in eWAT and displayed an inverse correlation with temperature. *Npr3* KO mice displayed enhanced mitochondrial function after cold exposure by increasing browning-related proteins and mitochondrial respiratory chain complexes expression and they resisted obesity induced by an HF/HS diet. The reduction in NPR-C promoted the mitochondrial function of white adipocytes in a manner dependent on NPR-B signaling. The NPR-C-specific antagonist was able to mimic the phenotype seen in *Npr3* knockout mice. These data indicate that NPR-C holds promise as a potential target for treating obesity and metabolic diseases.

Adipose tissue serves as insulation and protection against systemic metabolic disorders. Previous studies found that eWAT exhibits a higher inflammatory profile compared to sWAT (36). Moreover, during

obesity, eWAT not only undergoes hypertrophy (increase in size) but also becomes more hyperplastic than sWAT (37). In obese patients, the rapid expansion of eWAT is positively associated with an increased probability of cardiovascular disease (38). Therefore, the expansion of eWAT in obesity is far more harmful to the body than that of sWAT. Interestingly, we found that NPR-C expression was higher in eWAT compared to sWAT. Cold exposure is an effective way to induce adipose tissue browning by enhancing mitochondrial content and metabolic rate (39, 40). We found cold exposure decreased NPR-C expression. In *Npr3* knockout mice, the protection against obesity was more pronounced in eWAT than in sWAT. These data suggest that NPR-C plays a pivotal role in regulating eWAT.

In recent years, NP families have been discovered to have novel physiological functions in lipolysis, lipid oxidation, and mitochondrial respiration (41). ANP and CNP increase the expression of UCPI, a protein involved in energy dissipation, and also activate the mechanisms that promote overall mitochondrial biogenesis (6, 8). Members of the NP family significantly impact adipose tissue function, mediated through NPRs, particularly NPR-C. In this study, we observed that *Npr3* KO mice were leaner and resistant to HF/HS-induced obesity, consistent with previous studies (6, 17). These findings align with the role of CNP, which can bind to either NPR-B or NPR-C, as CNP KO mice exhibited phenotypes similar to those of *Npr3* KO mice (8, 42). Recently, a study reported that NPR-C can form heterodimers with NPR-A or NPR-B (12). We found that knockdown of *Npr3* promotes mitochondrial function by regulating NPR-B signaling, dependent on cGMP and calcium signaling. CNP effectively initiated the thermogenesis program in both mouse and human adipocytes by means of p38 MAPK activation (6). Moreover, activation of the AKT pathway promotes energy expenditure and protects against obesity (43). We demonstrated that blocking NPR-B signaling reduces the activation of p38 MAPK and AKT pathways caused by *Npr3* knockdown. In conclusion, our findings highlight that the crosstalk between NPR-C and NPR-B regulates mitochondrial function.

Mitochondria are crucial for cellular energy production, energy metabolism, and various cellular processes (44). PPAR signaling plays an essential role in regulating adipocyte thermogenesis (45, 46). In this study, RNA-sequencing data demonstrated that PPAR signaling was significantly activated in *Npr3* KO mice compared with WT mice after cold exposure, proving that NPR-C deficiency stimulated thermogenesis through multiple pathways, including PPAR signaling. PPARs are nuclear hormone receptors that regulate the expression of genes involved in energy metabolism (47). A key downstream target of PPAR signaling is

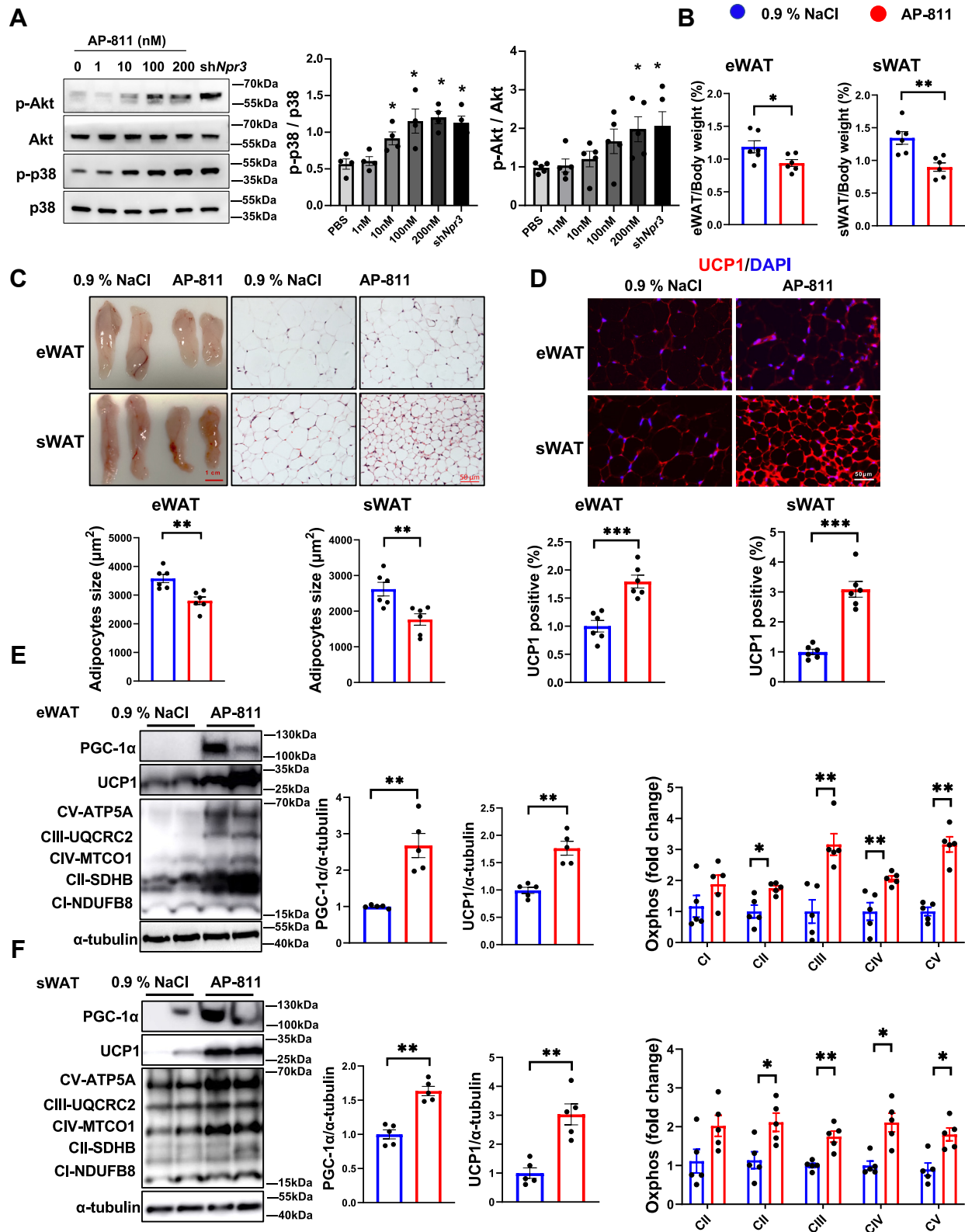


**Fig. 7.** Inhibition of NPR-C mimics cold-induced adipose tissue thermogenesis. **A:** Western blot analysis and quantification data of p-Akt/Akt and p-p38/p38 expression in SVF-induced white adipocytes under different doses of AP-811 for 5 min. **B:** Relative eWAT and sWAT weight of WT mice injected with 0.9% NaCl or AP-811. **C:** Representative images and H&E staining and adipocyte sizes of eWAT and sWAT. **D:** Representative images of uncoupling protein 1 (UCP1) (red) immunofluorescence and quantification data of eWAT and sWAT. DAPI was used to stain the nucleus in blue. **E:** Western blot analysis and quantification data of PGC1 $\alpha$ , UCP1, and mitochondrial respiratory chain complex expression in eWAT and sWAT. Data were analyzed by unpaired Student's *t*-test. \* $P < 0.05$ , \*\* $P < 0.01$ , \*\*\* $P < 0.001$ .

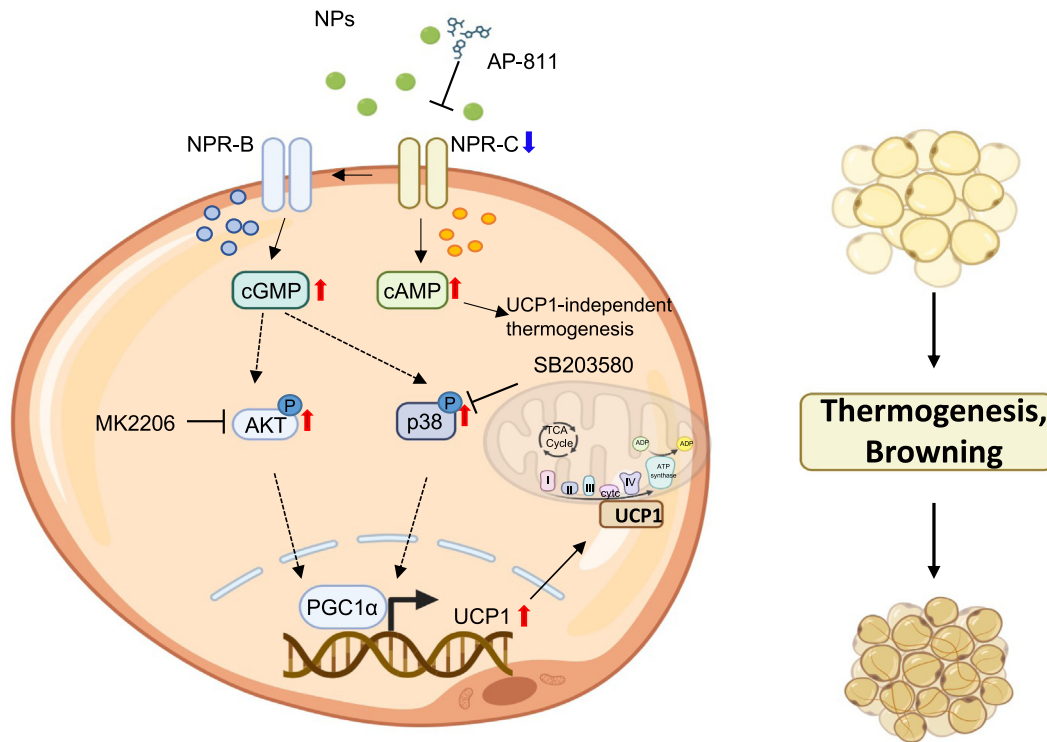


**Fig. 8.** Schematic representation of the mechanism of NPR-C on mitochondrial respiration in white adipose tissue.

PGC1 $\alpha$ , a transcriptional coactivator crucial for mitochondrial biogenesis and function (47). In WAT, PGC1 $\alpha$  increases UCP1 levels and up-regulates genes in the mitochondrial respiratory chain complexes, resembling the function of brown adipocytes (48, 49). In this context, our research demonstrated that NPR-C deficiency enhanced the expression of mitochondrial respiratory chain complex-related genes and improved mitochondrial function in WAT. This finding suggests that NPR-C plays a novel regulatory role in modulating PGC1 $\alpha$  and UCP1 expression, impacting overall mitochondrial energy dynamics in adipose tissues. This regulation appears to be especially prominent under conditions of cold exposure and is equivalent to the activation of the  $\beta$ 3-adrenergic receptor. More importantly, inhibition of NPR-C signaling in WT mice was sufficient to mimic the phenotype of *Npr3* KO mice. These insights open new avenues for therapeutic strategies targeting NPR-C to enhance mitochondrial efficiency and overall metabolic health in adipose tissues.

UCP1-independent thermogenesis also plays a key role in regulating adipocyte function, (50) including creatine cycling (51) and Ca<sup>2+</sup> cycling (50). Previous studies have shown that an increase in cytoplasmic calcium concentration and creatine levels can enhance mitochondrial thermogenesis in adipocytes (52, 53). While many UCP1-independent fat thermogenic pathways are regulated by the cAMP pathway, (54) which is activated by *Npr3* knockdown (55). Our study demonstrated that NPR-C deficiency increased intracellular

Ca<sup>2+</sup> levels. However, further studies are necessary to explore the role of NPR-C in UCP1-independent thermogenesis more thoroughly.

The limitation of this study lies in the heterogeneity of SVF cells, which include various cell types. According to the Human Cell Atlas, NPR-C is expressed in fibroblasts, adipocytes, and B cells within adipose tissue. Therefore, a conditional knockout approach is more informative in assessing the specific role of NPR-C in WAT homeostasis. Further investigation is warranted to elucidate NPR-C's specific roles in distinct adipose cell types.

In conclusion, our findings show that blocking NPR-C signaling can effectively improve metabolic diseases. The involvement of NPR-C in adipose tissue function is mediated through NP receptors by impacting mitochondrial function and potentially through the modulation of downstream signaling pathways.

#### Data availability

Data are available from the authors on request.

#### Supplemental data

This article contains [supplemental data](#).

#### Author contributions

S. L., X. L., J. W., R. W., and J. Z. data curation; S. L., J. W., and R. W. formal analysis; S. L., X. L., J. W., R. W., and Q. D. investigation; S. L., X. L., J. W., W. R., R. W., Q. D., and J. Z. methodology; S. L., X. L., J. W., P. G., and J. W. project



administration; S. L. and J. W. software, S. L., J. W., P. G., and J. W. supervision; S. L., J. W., and W. R. validation; S. L., J. W., and W. R. visualization; S. L., X. L., and J. W. writing—original draft; S. L., X. L., and J. W. writing—review & editing; X. L., Q. D., and J. W. conceptualization; X. L., Y. K., P. G., and J. W. funding acquisition; Y. K., J. W., P. G., and J. W. resources.

#### Author ORCIDs

Yuan-Yuan Kang  <https://orcid.org/0000-0001-9121-5872>

#### Funding and additional information

This study received financial support from the National Natural Science Foundation of China (82030006, 82070435, 82370426), the National Key R&D Program of China (2022YFA1104200), and the Shanghai Municipal Commissions of Science and Technology (21ZR1454100).

#### Conflict of interest

The authors declare that they have no conflict of interest with the contents of this article.

#### Abbreviations

AT, adipose tissue; NPR-C, Natriuretic peptide receptor-C; SVF, stromal vascular fraction; WAT, white adipose tissue.

Manuscript received March 6, 2024, and in revised form July 15, 2024. Published, JLR Papers in Press, August 19, 2024, <https://doi.org/10.1016/j.jlr.2024.100623>

## REFERENCES

- Morigny, P., Boucher, J., Arner, P., and Langin, D. (2021) Lipid and glucose metabolism in white adipocytes: pathways, dysfunction and therapeutics. *Nat. Rev. Endocrinol.* **17**, 276–295
- Tchernof, A., and Despres, J. P. (2013) Pathophysiology of human visceral obesity: an update. *Physiol. Rev.* **93**, 359–404
- Karpe, F., and Pinnick, K. E. (2015) Biology of upper-body and lower-body adipose tissue-link to whole-body phenotypes. *Nat. Rev. Endocrinol.* **11**, 90–100
- Borgeson, E., Boucher, J., and Hagberg, C. E. (2022) Of mice and men: pinpointing species differences in adipose tissue biology. *Front. Cell Dev. Biol.* **10**, 1003118
- Verboven, K., Hansen, D., Jocken, J. W. E., and Blaak, E. E. (2017) Natriuretic peptides in the control of lipid metabolism and insulin sensitivity. *Obes. Rev.* **18**, 1243–1259
- Bordicchia, M., Liu, D., Amri, E. Z., Ailhaud, G., Dessi-Fulgheri, P., Zhang, C., et al. (2012) Cardiac natriuretic peptides act via p38 MAPK to induce the brown fat thermogenic program in mouse and human adipocytes. *J. Clin. Invest.* **122**, 1022–1036
- Wu, W., Shi, F., Liu, D., Ceddia, R. P., Gaffin, R., Wei, W., et al. (2017) Enhancing natriuretic peptide signaling in adipose tissue, but not in muscle, protects against diet-induced obesity and insulin resistance. *Sci. Signal.* **10**, eaam6870
- Perez-Tertero, C., Aubdool, A. A., Makwana, R., Sanger, G. J., Stimson, R. H., Chan, L. F., et al. (2022) C-type natriuretic peptide is a pivotal regulator of metabolic homeostasis. *Proc. Natl. Acad. Sci. U. S. A.* **119**, e2116470119
- Moro, C. (2016) Targeting cardiac natriuretic peptides in the therapy of diabetes and obesity. *Expert Opin. Ther. Targets.* **20**, 1445–1452
- Prickett, T. C., and E, A. E. (2020) Circulating products of C-type natriuretic peptide and links with organ function in health and disease. *Peptides.* **132**, 170363
- Moyes, A. J., and Hobbs, A. J. (2019) C-Type natriuretic peptide: a multifaceted paracrine regulator in the heart and vasculature. *Int. J. Mol. Sci.* **20**, 2281
- Liu, D., Ceddia, R. P., Zhang, W., Shi, F., Fang, H., and Collins, S. (2023) Discovery of another mechanism for the inhibition

- of particulate guanylyl cyclases by the natriuretic peptide clearance receptor. *Proc. Natl. Acad. Sci. U. S. A.* **120**, e2307882120
- Schmid, A., Albrecht, J., Brock, J., Koukou, M., Arapogianni, E., Schaffler, A., et al. (2018) Regulation of natriuretic peptides postprandially in vivo and of their receptors in adipocytes by fatty acids in vitro. *Mol. Cell Endocrinol.* **473**, 225–234
- Zhu, Q., An, Y. A., and Scherer, P. E. (2022) Mitochondrial regulation and white adipose tissue homeostasis. *Trends Cell Biol.* **32**, 351–364
- Wu, J., Bostrom, P., Sparks, L. M., Ye, L., Choi, J. H., Giang, A. H., et al. (2012) Beige adipocytes are a distinct type of thermogenic fat cell in mouse and human. *Cell.* **150**, 366–376
- Guo, W., Jiang, L., Bhasin, S., Khan, S. M., and Swerdlow, R. H. (2009) DNA extraction procedures meaningfully influence qPCR-based mtDNA copy number determination. *Mitochondrion.* **9**, 261–265
- Chen, H. J., Zhang, W. X., Hu, L., Fan, J., Zhang, L., and Yan, Y. E. (2020) Maternal nicotine exposure enhances adipose tissue angiogenic activity in offspring: sex and age differences. *Toxicology.* **441**, 152506
- Huang, Z., and Xu, A. (2021) Adipose extracellular vesicles in intercellular and inter-organ crosstalk in metabolic health and diseases. *Front. Immunol.* **12**, 608680
- Reinisch, I., Schreiber, R., and Prokesch, A. (2020) Regulation of thermogenic adipocytes during fasting and cold. *Mol. Cell Endocrinol.* **512**, 110869
- Barquissau, V., Leger, B., Beuzelin, D., Martins, F., Amri, E. Z., Pisani, D. F., et al. (2018) Caloric restriction and diet-induced weight loss do not induce browning of human subcutaneous white adipose tissue in women and men with obesity. *Cell Rep.* **22**, 1079–1089
- Maffei, C., Schutz, Y., Grezzani, A., Provera, S., Piacentini, G., and Tato, L. (2001) Meal-induced thermogenesis and obesity: is a fat meal a risk factor for fat gain in children? *J. Clin. Endocrinol. Metab.* **86**, 214–219
- Shao, S., Li, X. D., Lu, Y. Y., Li, S. J., Chen, X. H., Zhou, H. D., et al. (2021) Renal natriuretic peptide receptor-C deficiency attenuates NaCl cotransporter activity in angiotensin II-induced hypertension. *Hypertension.* **77**, 868–881
- Matsukawa, N., Grzesik, W. J., Takahashi, N., Pandey, K. N., Pang, S., Yamauchi, M., et al. (1999) The natriuretic peptide clearance receptor locally modulates the physiological effects of the natriuretic peptide system. *Proc. Natl. Acad. Sci. U. S. A.* **96**, 7403–7408
- Jash, S., Banerjee, S., Lee, M. J., Farmer, S. R., and Puri, V. (2019) CIDEA transcriptionally regulates UCPI for browning and thermogenesis in human fat cells. *iScience.* **20**, 73–89
- Rooney, J. P., Ryde, I. T., Sanders, L. H., Howlett, E. H., Colton, M. D., Germ, K. E., et al. (2015) PCR based determination of mitochondrial DNA copy number in multiple species. *Methods Mol. Biol.* **1241**, 23–38
- Hajer, G. R., van Haften, T. W., and Visseren, F. L. (2008) Adipose tissue dysfunction in obesity, diabetes, and vascular diseases. *Eur. Heart J.* **29**, 2959–2971
- Liu, Y., Li, M., Lv, X., Bao, K., Yu Tian, X., He, L., et al. (2022) Yes-associated protein targets the transforming growth factor beta pathway to mediate high-fat/high-sucrose diet-induced arterial stiffness. *Circ. Res.* **130**, 851–867
- Bulthuis, E. P., Dieteren, C. E. J., Bergmans, J., Berkhout, J., Wagenaars, J. A., van de Westerlo, E. M. A., et al. (2023) Stress-dependent macromolecular crowding in the mitochondrial matrix. *EMBO J.* **42**, e108533
- Chaurasia, B., Kaddai, V. A., Lancaster, G. I., Henstridge, D. C., Sriram, S., Galam, D. L., et al. (2016) Adipocyte ceramides regulate subcutaneous adipose browning, inflammation, and metabolism. *Cell Metab.* **24**, 820–834
- Cao, X., Shi, T. T., Zhang, C. H., Jin, W. Z., Song, L. N., Zhang, Y. C., et al. (2022) ACE2 pathway regulates thermogenesis and energy metabolism. *Elife.* **11**, e72266
- Zhang, Y., Xue, J., Zhu, W., Wang, H., Xi, P., and Tian, D. (2024) TRPV4 in adipose tissue ameliorates diet-induced obesity by promoting white adipocyte browning. *Transl. Res.* **266**, 16–31
- Leiva, M., Matesanz, N., Pulgarin-Alfaro, M., Nikolic, I., and Sabio, G. (2020) Uncovering the role of p38 family Members in adipose tissue physiology. *Front. Endocrinol. (Lausanne).* **11**, 572089



33. Lafontan, M., Moro, C., Berlan, M., Crampes, F., Sengenès, C., and Galitzky, J. (2008) Control of lipolysis by natriuretic peptides and cyclic GMP. *Trends Endocrinol. Metab.* **19**, 130–137
34. Gruden, G., Landi, A., and Bruno, G. (2014) Natriuretic peptides, heart, and adipose tissue: new findings and future developments for diabetes research. *Diabetes Care.* **37**, 2899–2908
35. Neeland, I. J., Winders, B. R., Ayers, C. R., Das, S. R., Chang, A. Y., Berry, J. D., *et al.* (2013) Higher natriuretic peptide levels associate with a favorable adipose tissue distribution profile. *J. Am. Coll. Cardiol.* **62**, 752–760
36. Emont, M. P., Jacobs, C., Essene, A. L., Pant, D., Tenen, D., Colletuori, G., *et al.* (2022) A single-cell atlas of human and mouse white adipose tissue. *Nature.* **603**, 926–933
37. Vijay, J., Gauthier, M. F., Biswell, R. L., Louiselle, D. A., Johnston, J. J., Cheung, W. A., *et al.* (2020) Single-cell analysis of human adipose tissue identifies depot and disease specific cell types. *Nat. Metab.* **2**, 97–109
38. Powell-Wiley, T. M., Poirier, P., Burke, L. E., Despres, J. P., Gordon-Larsen, P., Lavie, C. J., *et al.* (2021) Obesity and cardiovascular disease: a scientific statement from the American heart association. *Circulation.* **143**, e984–e1010
39. Greenhill, C. (2017) Adipose tissue: towards mimicking cold exposure. *Nat. Rev. Endocrinol.* **13**, 316
40. Lim, S., Honek, J., Xue, Y., Seki, T., Cao, Z., Andersson, P., *et al.* (2012) Cold-induced activation of brown adipose tissue and adipose angiogenesis in mice. *Nat. Protoc.* **7**, 606–615
41. Schlueter, N., de Sterke, A., Willmes, D. M., Spranger, J., Jordan, J., and Birkenfeld, A. L. (2014) Metabolic actions of natriuretic peptides and therapeutic potential in the metabolic syndrome. *Pharmacol. Ther.* **144**, 12–27
42. Sogawa-Fujiwara, C., Hanagata, A., Fujiwara, Y., Ishida, Y., Tomiyasu, H., Kunieda, T., *et al.* (2020) Defective development and microcirculation of intestine in Npr2 mutant mice. *Sci. Rep.* **10**, 14761
43. Caratti, G., Stifel, U., Caratti, B., Jamil, A. J. M., Chung, K. J., Kiehnopf, M., *et al.* (2023) Glucocorticoid activation of anti-inflammatory macrophages protects against insulin resistance. *Nat. Commun.* **14**, 2271
44. Miao, Y., Wu, W., Dai, Y., Maneix, L., Huang, B., Warner, M., *et al.* (2015) Liver X receptor beta controls thyroid hormone feedback in the brain and regulates browning of subcutaneous white adipose tissue. *Proc. Natl. Acad. Sci. U. S. A.* **112**, 14006–14011
45. Shen, H., He, T., Wang, S., Hou, L., Wei, Y., Liu, Y., *et al.* (2022) SOX4 promotes beige adipocyte-mediated adaptive thermogenesis by facilitating PRDM16-PPARgamma complex. *Theranostics.* **12**, 7699–7716
46. Zhang, Z., Cui, Y., Su, V., Wang, D., Tol, M. J., Cheng, L., *et al.* (2023) A PPARgamma/long noncoding RNA axis regulates adipose thermoneutral remodeling in mice. *J. Clin. Invest.* **133**, e170072
47. Jamwal, S., Blackburn, J. K., and Elsworth, J. D. (2021) PPARgamma/PGC1alpha signaling as a potential therapeutic target for mitochondrial biogenesis in neurodegenerative disorders. *Pharmacol. Ther.* **219**, 107705
48. Puigserver, P., Wu, Z., Park, C. W., Graves, R., Wright, M., and Spiegelman, B. M. (1998) A cold-inducible coactivator of nuclear receptors linked to adaptive thermogenesis. *Cell.* **92**, 829–839
49. Tiraby, C., Tavernier, G., Lefort, C., Larrouy, D., Bouillaud, F., Ricquier, D., *et al.* (2003) Acquisition of brown fat cell features by human white adipocytes. *J. Biol. Chem.* **278**, 33370–33376
50. Ikeda, K., Kang, Q., Yoneshiro, T., Camporez, J. P., Maki, H., Homma, M., *et al.* (2017) UCPI-independent signaling involving SERCA2b-mediated calcium cycling regulates beige fat thermogenesis and systemic glucose homeostasis. *Nat. Med.* **23**, 1454–1465
51. Rahbani, J. F., Bunk, J., Lagarde, D., Samborska, B., Roesler, A., Xiao, H., *et al.* (2024) Parallel control of cold-triggered adipocyte thermogenesis by UCPI and CKB. *Cell Metab.* **36**, 526–540.e7
52. Guarnieri, A. R., Benson, T. W., and Tranter, M. (2022) Calcium cycling as a mediator of thermogenic metabolism in adipose tissue. *Mol. Pharmacol.* **102**, 51–59
53. Kazak, L., Chouchani, E. T., Jedrychowski, M. P., Erickson, B. K., Shinoda, K., Cohen, P., *et al.* (2015) A creatine-driven substrate cycle enhances energy expenditure and thermogenesis in beige fat. *Cell.* **163**, 643–655
54. Rahbani, J. F., Roesler, A., Hussain, M. F., Samborska, B., Dykstra, C. B., Tsai, L., *et al.* (2021) Creatine kinase B controls futile creatine cycling in thermogenic fat. *Nature.* **590**, 480–485
55. Meng, L., Lu, Y., Wang, X., Cheng, C., Xue, F., Xie, L., *et al.* (2023) NPRC deletion attenuates cardiac fibrosis in diabetic mice by activating PKA/PKG and inhibiting TGF-beta1/Smad pathways. *Sci. Adv.* **9**, eadd4222